Supporting Information

Physics-based bias-dependent compact modeling of *1/f* noise in single- to few- layer 2D-FETs

Nikolaos Mavredakis[*a], Anibal Pacheco-Sanchez[a], Md Hasibul Alam[b], Anton Guimerà-Brunet[c, d], Javier Martinez[c], Jose Antonio Garrido[e, f], Deji Akinwande[b] and David Jiménez[a]*

[a] *Departament d'Enginyeria Electrònica, Escola d'Enginyeria, Universitat Autònoma de Barcelona, Bellaterra 08193, Spain*

[b] *Department of Electrical and Computer Engineering, The University of Texas, Austin, TX 78758, USA*

[c] *Instituto de Microelectrónica de Barcelona, IMB-CNM (CSIC), Esfera UAB, Bellaterra, Spain*

[d] *Centro de Investigación Biomédica en Red en Bioingenieria, Biomateriales y Nanomedicina (CIBER-BBN), Madrid, Spain*

[e] *Catalan Institute of Nanoscience and Nanotechnology (ICN2), CSIC, Barcelona Institute of Science and Technology, Campus UAB, Bellaterra, Barcelona, Spain*

[f] *ICREA, Pg. Lluis Companys 23, 08010 Barcelona, Spain*

* *Email: nikolaos.mavredakis@uab.cat*

SECTION S.1 Definitions of basic quantities of the *IV* model

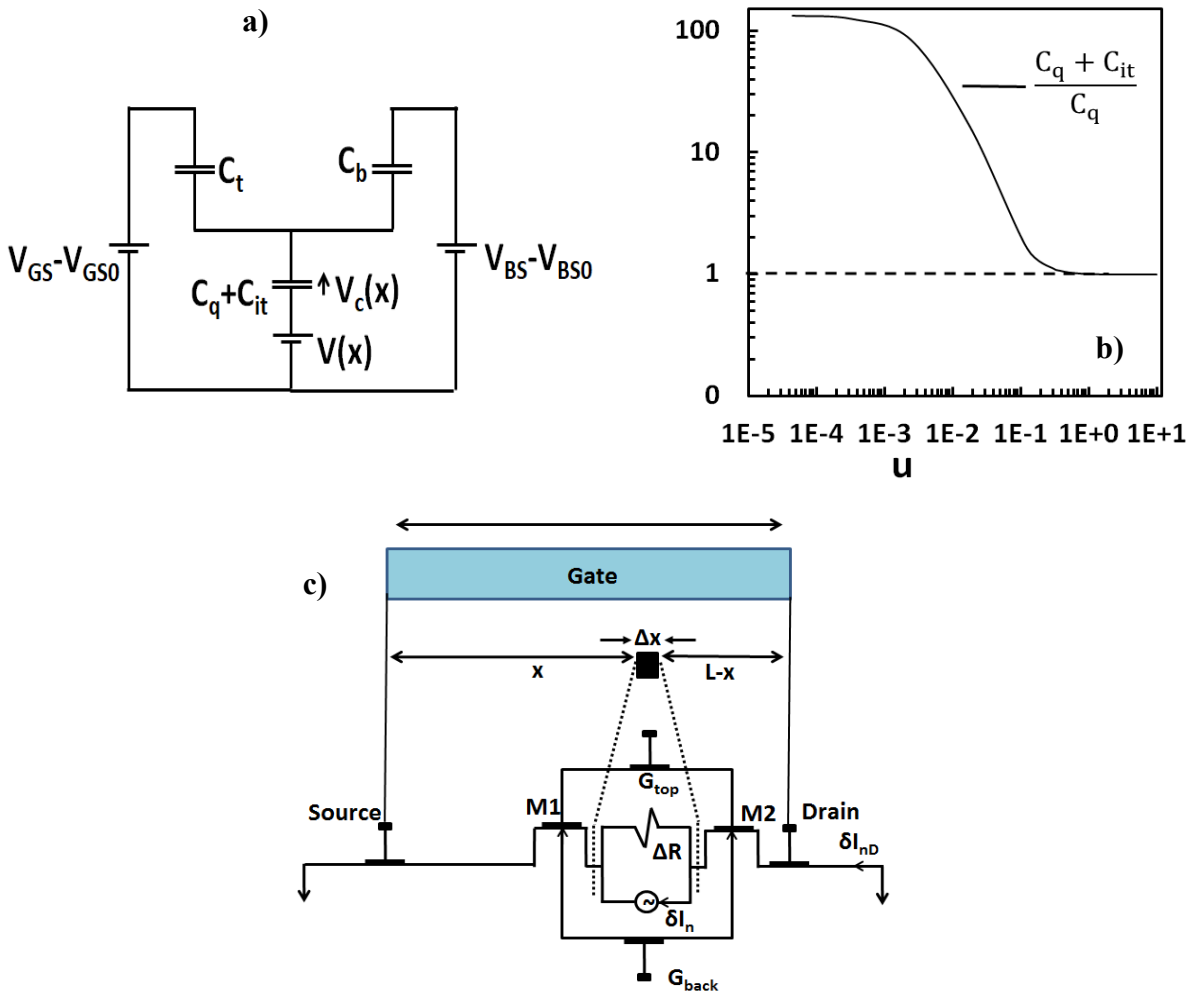

Fig. S1. a) Capacitive circuit of a 2D-FET, b) quantum-interface trap capacitance related term $(C_q+C_{it})/C_q$ vs. normalized charge u and c) the equivalent circuit for a local current noise contribution to the total noise is illustrated. Each noise-generating slice of the channel is connected to two noiseless 2D-FETs, M1 and M2 respectively.

Notice that as mentioned in the main manuscript, we present equations for n-type 2DFETs to simplify the analysis which can be easily adjusted to p-type devices.[63] Fig. S1a depicts the

equivalent capacitive circuit of the *CV-IV* chemical potential (V_c) based model[63] from where the basic electrostatics can be derived as:[57-58, 63]

$$-Q_{2D}(x)-Q_{it}(x)=C_t(V_{GS}-V_{GS0}-\psi(x))+C_b(V_{BS}-V_{BS0}-\psi(x)) \quad \text{(S1)}$$

where Q_{2D} is the overall net mobile sheet, $Q_{it}(x)$ is the interface trap charge, $C_{t,b}$ is the top(back)-dielectric capacitance per unit area, while $V_{G(S)B}$ is the top(back)-gate voltage with $V_{G(S)B0}$ the flat band top(back)-gate voltage[63]. Ψ is the electrostatic potential with $\psi(x)=V(x)+V_c(x) \leftrightarrow e.V_c(x)=-e.V(x)+e.\psi(x)=E_F(x)-E_C(x)$[57-58] where V is the channel potential and $V_c(x)$ symbolizes the shift of the quasi-fermi level $E_F(x)$ with $E_c(x)$ the conduction band edge, e the electron charge and x the channel position; $V(x=0)=V_S$, $V_c(x=0)=V_{cs}$ at source side and $V(x=L)=V_D$, $V_c(x=L)=V_{cd}$ at drain side, respectively.[57-58, 63]. Q_{2D} is defined as:[63]

$$Q_{2D}(x)=-C_{dq}U_T u(V_c),\ \ u(V_c)=ln\left(1+e^{\frac{V_c}{U_T}}\right) \quad \text{(S2)}$$

where U_T is the thermal voltage, u is a normalized charge term, $C_{dq}=e^2.D_{oS}$ is the degenerated quantum capacitance, which corresponds to its upper-limit value when the carrier density becomes heavily degenerated; $D_{oS}=g_k.m^k/(2\pi.h^2)+g_Q.m^Q/(2\pi.h^2)e^{[\Delta E2/KT]}$ is the 2D density of states with h the reduced Planck constant $(=1.05\cdot10^{-34}\ J.s)$, $g_{k,Q}$ the degeneracy factor and $m^{k,Q}$ the conduction band effective mass at the k, Q band valley, respectively where $\Delta E2$ is the energy separation between k, Q bands, K the Boltzmann constant and T the temperature[58, 60, 63]. $V_{cs(d)}$ at source (drain) side, can be derived from Equations S1-S2 after applying a self-consistent solution.[63] Quantum capacitance C_q is defined as the derivative of Q_{2D} over V_c ($C_q=-dQ_{2D}/dV_c$[58, 63]) and after expanding the later by considering Equation S2:

$$C_q=\frac{-dQ_{2D}}{dV_c}=\frac{-dQ_{2D}\,du}{du\quad dV_c}=C_{dq}\frac{e^{V_{C/U_T}}}{(1+e^{V_{C/U_T}})} \quad \text{(S3)}$$

$$u(V_C)=ln\left(1+e^{V_{C/U_T}}\right)\rightarrow e^{V_{C/U_T}}=e^u-1 \quad \text{(S4)}$$

and thus, from Equations S3-S4:

$$C_q=C_{dq}\frac{e^u-1}{e^u}=C_{dq}(1-e^{-u}),\frac{dV_c}{du}=\frac{C_{dq}U_T}{C_q} \quad \text{(S5)}$$

From Equation S1:

$$\frac{d\psi}{dV_c}=-\frac{C_q+C_{it}}{C}\rightarrow\frac{d(V+V_c)}{dV_c}=\frac{C_q+C_{it}}{C}\rightarrow\frac{dV}{dV_c}=-\frac{C_q}{C}-1=-\left(\frac{C_q+C_{it}+C}{C}\right) \quad \text{(S6)}$$

where $C=C_t+C_b$ and $C_{it}=-dQ_{it}/dV_c$ is the interface trap capacitance[58, 63]. From Drift-Diffusion I_D definition[63] and from Equations S3-S6:

$$I_D = -W|Q_{2D}|\mu_{eff}E = W|Q_{2D}|\frac{\mu \quad dV}{1+\frac{\mu}{v_{sat}}|-d\psi|dx} \Rightarrow I_D\left[1+\frac{\mu}{v_{sat}}\left|-\frac{d\psi}{dV_c}\frac{dV_c du}{du\,dx}\right|\right] = W|Q_{2D}|\mu\frac{dV}{dV_c}\frac{dV_c du}{du\,dx} =$$

$$= -W|Q_{2D}|\mu\frac{C_q + C_{it} + CC_{dq}U_T du}{C \quad C_q \quad dx} \Rightarrow -W|Q_{2D}|\mu\frac{C_q + C_{it} + CC_{dq}U_T du}{C \quad C_q \quad dx} - I_D\frac{\mu}{v_{sat}}\frac{C_{dq}U_T C_q + C_{it}}{C \quad C_q}$$

$$\frac{|du|du}{du\,dx} = I_D \Rightarrow \frac{dx}{du} = -\frac{W|Q_{2D}|\mu C_q + C_{it} + CC_{dq}U_T}{I_D \quad C \quad C_q} - \frac{\mu}{v_{sat}}\frac{C_{dq}U_T|du|}{C \quad du}$$

(S7)

where μ_{eff} is the effective mobility after the degradation of low-field mobility μ due to velocity saturation (VS) effect and $E=-dV/dx$, $E_x=-d\psi/dx$, $E_c=u_{sat}/\mu$ represent the electric, horizontal and critical electric fields, respectively. The second term in penultimate line of Equation S7 is related with VS effect which becomes significant at elevated gate and drain voltages ($V_{GS(B)}$, V_{DS}), respectively[54-55] for 2D-FETs. Under such operating conditions, C_q dominates over C_{it} and hence, $(C_q+C_{it})/C_q \approx 1$ at high charge density regime as presented in Fig. S1b. This approximation is applied in this VS-related term of Equation S7 as it is displayed in its last line. The *IV* parameters used for the simulations in Fig. S1b, are adapted from the DUT measured in the present study (cf. row 3 of Table S1 in Section S.6) but the same outcome is obtained for other parameters sets.[33, 35, 38, 40, 42-43, 49] If we multiply both terms of final expression of Equation S7 with du and integrate from source to drain we get:

$$I_D = \frac{\int_{u_s}^{u_d} -W|Q_{2D}|\mu C_{dq}U_T\frac{C_q + C_{it} + C}{C_q C}du}{L + \frac{\mu C_{dq}U_T}{u_{sat}C}\int_{u_s}^{u_d}|du|} = \frac{\frac{W\mu(C_{dq}U_T)^2}{C}\int_{u_d}^{u_s} u\frac{C_q + C_{it} + C}{C_q}du}{L + \frac{\mu C_{dq}U_T}{u_{sat}C}|u_d - u_s|}$$

(S8)

where u_s, u_d are the source and drain side normalized charges, respectively, which can be easily calculated from Equation S2 after V_{cs}, V_{cd} derivation. The denominator of Equation S8 corresponds to an effective effect L_{eff} that accounts for VS effect[52-53] while the numerator can be expanded as:

$$I_D = \frac{W\mu(C_{dq}U_T)^2}{CL_{eff}}\left[\int_{u_d}^{u_s} u\frac{C_q + C}{C_q}du + \int_{u_d}^{u_s} u\frac{C_{it}}{C_q}du\right]$$

(S9)

where the first term in the brackets of Equation S9 has already been solved and used in the *IV* model[63 (Equation 5)] and is given by:

$$I_{DA} = \frac{W\mu(C_{dq}U_T)^2}{CL_{eff}}\int_{u_d}^{u_s} u\frac{C_q + C}{C_q}du = \frac{W\mu C_{dq}U_T^2}{L_{eff}}\left[\left(\frac{C_{dq} + C}{C}\right)\left(\frac{u_s^2 - u_d^2}{2}\right) + e^{-u_d} - e^{-u_s}\right]$$

(S10a)

while the second term equals to:

$$I_{DB} = \frac{W\mu(C_{dq}U_T)^2}{CL_{eff}}\int_{u_d}^{u_s} u\frac{C_{it}}{C_q}du = \frac{W\mu C_{dq}U_T^2 C_{it}}{CL_{eff}}\int_{u_d}^{u_s}\frac{u}{1-e^{-u}}du = \frac{W\mu C_{dq}U_T^2 C_{it}}{CL_{eff}}\left[uln(1-e^u)+Li_2(e^u)\right]_{u_d}^{u_s} \approx \left[\left(\frac{u_s^2-u_d^2}{2}\right)+e^{-u_d}-e^{-u_s}\right] \quad \text{(S10b)}$$

Notice firstly that C_{it}/C_q integral in Equation S10b cannot be solved analytically thus, we approximate a uniform channel condition (low V_{DS}) for C_{it} which is then considered equal to its value at source side ($V_c(x)=V_{cs}$) all along the channel, $C_{it}=e.N_{it}/(2U_T.(1+cosh[(-V_{cs}-V_{it})/U_T]))$[63], and thus, can be taken out of the integral leading to a compact formulation; N_{it}, V_{it} are the effective interface trap density and energy, respectively used as *IV* model parameters[63]. Secondly, Li_2 denotes the polylogarithm function of the second order and Equation S10b is solved after similar treatment with Equation S10a (cf. Equations 26-29 in Appendix of Ref. 60). Thus, the new more complete I_D expression is:

$$I_D = I_{DA} + I_{DB} = \frac{\mu W C_{dq}U_T^2}{L_{eff}}gvc, \quad gvc = \left[\frac{C_{dq}+C_{it}+Cu_s^2-u_d^2}{C \quad 2}+\frac{C_{it}+C}{C}\left(e^{-u_d}-e^{-u_s}\right)\right] \quad \text{(S11)}$$

Equation S7 becomes due to Equation S11:

$$\frac{dx}{du} = -|Q_{2D}|\frac{L_{eff}}{CU_T gvc}\frac{C_q+C_{it}+C}{C_q} - \frac{\mu}{v_{sat}}\frac{C_{dq}U_T|du|}{C \quad du} \quad \text{(S12)}$$

which defines the relation between *du* and *dx* which will be proved very beneficial for the *1/f* noise derivations in the next Section.

SECTION S.2 Secondary *IV* effects included in the model

The *IV* model that is used in this work[63] has not contained until now various effects that can affect the experimental *IV* data. Such effects are: a) the V_{DS} dependence of threshold voltage-V_{TH} (Drain Induced Barrier Lowering-DIBL), b) the V_{DS} dependence of contact resistance and c) the Channel Length Modulation (CLM) effect. Regarding DIBL, the following expression is added:[61] $V_{TH}=V_{G(S)B0}-n_{DIBL}V_{DS}$ where n_{DIBL} (unitless) is a model parameter. The subsequent equation has also been implemented to describe the V_{DS} dependence of contact resistance:[61] $R_{CS,D}=R_{CA}+R_{CB}V_{DS}^{bRC}$ where $R_{CS,D}$ is the contact resistance at source and drain side, respectively and R_{CA} (Ω), R_{CB} (Ω/V), bR_C (unitless) are used as model parameters. Finally, CLM has been included as:[58] $I_{D,CLM}=I_D(1+\lambda V_{DS})$ where $I_{D,CLM}$ is the drain current after the effect of CLM and λ ($1/V$) is a model parameter.

SECTION S.3 Thorough procedure for *1/f* noise derivations

As described in Ref. 27 (Section 6.1.1), the adopted methodology for *1/f* noise derivations, considers a noiseless channel apart from an elementary slice between *x* and *x+Δx* as shown in Fig. S1c. This local noise contribution can be represented by a local current noise source with a Power Spectral Density (PSD) $S_{\delta I}{}^2{}_n$ which is connected in parallel with the resistance ΔR of the slice. The transistor then can be split into two noiseless transistors M1 and M2 on each

side of the local current noise source, at the source and drain side ends with channel lengths equal to *x* and *L-x* respectively. Since the voltage fluctuations on parallel resistance *ΔR* are small enough compared to U_T, small signal analysis can be used in order to extract a noise model according to which, M1 and M2 can be replaced by two simple conductances G_S on the source and G_D on the drain side, respectively. The PSD of the drain current fluctuations $S_{\delta I^2 nD}$ due to a single local noise source is given by:[27] (Equation 6.3)

$$S_{\delta I_{nD}^{\ 2}}(\omega,x) = G_{CH}^2 \Delta R^2 S_{\delta I_n^2}(\omega,x) \tag{S13}$$

where *ω* is the angular frequency and G_{GH} is the channel conductance at *x* where:[27] (Equation 6.2)

$$\frac{1}{G_{CH}} = \frac{1}{G_S} + \frac{1}{G_D} \tag{S14}$$

Total drain current noise PSD along the channel is obtained by summing the elementary contributions $S_{\delta I^2 nD}$ in Equation S13 assuming that the contribution of each slice at different positions along the channel remains uncorrelated:[27] (Equations 6.4, 9.140)

$$S_{ID} = \int_0^L \frac{S_{\delta I_{nD}^{\ 2}}(\omega,x)}{\Delta x} dx = \int_0^L G_{CH}^2 \Delta R^2 \frac{S_{\delta I_n^2}(\omega,x)}{\Delta x} dx = \int_0^L \left(\frac{W\mu_{eff}Q_{2D}}{L_{eff}} \frac{\Delta x}{W\mu_{eff}Q_{2D}}\right)^2 \frac{S_{\delta I_n^2}(\omega,x)}{\Delta x} dx = \frac{1}{L_{eff}^2} \int_0^L \Delta$$
$$dx \tag{S15}$$

Regarding Carrier Number Fluctuation effect (*ΔN*), the fluctuation of the trapped charge δQ_t (containing slow border traps that contribute to *1/f* noise) can cause an alteration in the chemical potential δV_c which results in a variation of all the charges that depend directly on V_c (top(back)-dielectric charge $Q_{top(back)}$, Q_{2D} and Q_{it}). By applying charge conservation law[27] (Equations 6.56-6.57)-28, 52 and by considering C_q, C_{it} aforementioned definitions:

$$\delta Q_{2D} + \delta Q_{top} + \delta Q_{back} + \delta Q_{it} = \delta Q_t \rightarrow -(C_q \delta V_c + C_t \delta V_c + C_b \delta V_c + C_{it} \delta V_c) = \delta Q_t \rightarrow \frac{\delta Q_{2D}}{\delta Q_t} = \frac{C_q}{C_q + C + C_{it}} \tag{S16}$$

while relative current fluctuation equals, according to Equation S16, to:[27] (Equation 6.55)

$$\frac{\delta I_D(x)}{I_D} = \left(\frac{\delta N_{2D}}{N_{2D}\delta N_t} + \alpha_c e\mu\right)\delta \mathrm{N}_t = \left(\frac{e}{Q_{2D}} \frac{\delta Q_{2D}}{\delta Q_t} + \alpha_c e\mu\right)\delta \mathrm{N}_t = \left(\frac{e}{|Q_{2D}|} \frac{C_q}{C_q + C + C_{it}} + \alpha_c e\mu\right)\delta \mathrm{N}_t \tag{S17}$$

where α_c is the Coulomb scattering coefficient and N_{2D}, N_t are the net mobile and border trapped charge densities, respectively. Local *ΔN 1/f* noise is then calculated based on Equation S17 as:[27] (Equations 6.56-6.57, 6.64), 28, 52

$$\frac{S_{\delta I_n^2}}{I_D^2} f|_{\Delta \mathrm{N}} = \left(\frac{e}{|Q_{2D}|} \frac{C_q}{C_q + C + C_{it}} + \alpha_c e\mu\right)^2 S_{\delta N_t^2} \tag{S18}$$

where *f* is the frequency and $S_{\delta Nt^2} = KTN_{ST}/W\Delta xf$ the trap density fluctuation PSD[27] (Equation 6.65) with *W* the width of the device and N_{ST} the slow border trap density per unit energy in eV^{-}

$^{1}.cm^{-2}$; N_{ST} and α_c are used as *ΔN 1/f* noise model parameters. The first term in the right-hand parenthesis expresses the genuine carrier number fluctuation due to trapping/detrapping while the second signifies the correlated mobility fluctuation induced by the influence of trapping on Coulomb scattering mechanism (*CMF*).[27-32] Total *ΔN 1/f* noise normalized with squared drain current can be derived from Equations S15, S18 as:

$$\frac{S_{I_D}}{I_D^2} f|_{\Delta N} = \frac{KTN_{ST}}{WL_{eff}^2}\int_0^L \left(\frac{e}{Q_{2D}C_q + C_{it} + C}\frac{C_q}{} + \alpha_c e\mu\right)^2 dx = \frac{KTN_{ST}}{WL_{eff}^2}\left[\int_0^L \left(\frac{e}{|Q_{2D}|C_q + C_{it} + C}\frac{C_q}{}\right)^2 dx + \int_0^L (\alpha_c e\mu)^2 dx + \right. \quad \text{(S19)}$$

The integral in Equation S19 can be split into three integrals named *ΔN1*, *ΔN2* and *ΔN3* where *ΔN=ΔN1+ΔN2+ΔN3.* It is critical here to alter the integral variable from *x* to *u* (cf. Equation S12) in order to solve the integrals in a compact way as fundamental quantities of the *IV* model like Q_{2D}, C_q, which are contained in *1/f* noise derivations, are expressed in terms of *u*. *ΔN1* is calculated, if the aforementioned integral variable change is applied, as:

$$\Delta N1 = \frac{KTN_{ST}}{WL_{eff}^2}\int_{u_s}^{u_d}\left[\left(\frac{e}{|Q_{2D}|C_q + C_{it} + C}\frac{C_q}{}\right)^2\right]\left[-|Q_{2D}|\frac{L_{eff}}{CU_T gvc}\frac{C_q + C_{it} + C}{C_q} - \frac{\mu}{v_{sat}}\frac{C_{dq}U_T}{C}\frac{|du|}{du}\right]du \quad \text{(S20)}$$

where *ΔN1* is again divided into two integrals as *ΔN1=ΔN1A-ΔN1B*:

$$\Delta N1A = \frac{KTN_{ST}}{WL_{eff}^2}\int_{u_d}^{u_s}\left[\left(\frac{e}{|Q_{2D}|C_q + C_{it} + C}\frac{C_q}{}\right)^2\right]\left[|Q_{2D}|\frac{L_{eff}}{CU_T gvc}\frac{C_q + C_{it} + C}{C_q}\right]du \quad \text{(S21a)}$$

$$\Delta N1B = \frac{KTN_{ST}}{WL_{eff}^2}\int_{u_s}^{u_d}\left[\left(\frac{e}{|Q_{2D}|C_q + C_{it} + C}\frac{C_q}{}\right)^2\right]\left[\frac{\mu}{v_{sat}}\frac{C_{dq}U_T}{C}\right]|du| \quad \text{(S21b)}$$

ΔN2 is calculated as:

$$\Delta N2 = \frac{KTN_{ST}}{WL_{eff}^2}\int_0^L (\alpha_c e\mu)^2 dx = \frac{KTN_{ST}}{WL_{eff}^2}(\alpha_c e\mu)^2\int_0^L dx = \frac{KTN_{ST}L}{WL_{eff}^2}(\alpha_c e\mu)^2 \quad \text{(S22)}$$

and it does not require the integral variable change to be solved, as the quantity inside the integral area is constant and can be taken out. *ΔN3* is estimated, if the integral variable change presented in Equation S12 is applied, as:

$$\Delta N3 = \frac{KTN_{ST}}{WL_{eff}^2}\int_{u_s}^{u_d}\left[2\frac{\alpha_c e^2\mu}{|Q_{2D}|}\frac{C_q}{C_q + C_{it} + C}\right]\left[-|Q_{2D}|\frac{L_{eff}}{CU_T gvc}\frac{C_q + C_{it} + C}{C_q} - \frac{\mu}{v_{sat}}\frac{C_{dq}U_T}{C}\frac{|du|}{du}\right]du \quad \text{(S23)}$$

where *ΔN3* is again divided into two integrals as *ΔN3=ΔN3A-ΔN3B*:

$$\Delta N3A = \frac{KTN_{ST}}{WL_{eff}^2}\int_{u_d}^{u_s}\left[2\frac{\alpha_c e^2\mu}{|Q_{2D}|}\frac{C_q}{C_q + C_{it} + C}\right]\left[|Q_{2D}|\frac{L_{eff}}{CU_T gvc}\frac{C_q + C_{it} + C}{C_q}\right]du = \frac{2KTN_{ST}e^2\alpha_c\mu(u_s - u_d)}{WL_{eff}CU_T gvc} \quad \text{(S24a)}$$

$$\Delta N3B = \frac{KTN_{ST}}{WL_{eff}^2}\int_{u_s}^{u_d}\left[2\frac{\alpha_c e^2\mu}{|Q_{2D}|}\frac{C_q}{C_q + C_{it} + C}\right]\left[\frac{\mu}{v_{sat}}\frac{C_{dq}U_T}{C}\right]|du| \quad \text{(S24b)}$$

The integrals of Equations S21, S24b are presented below after considering Q_{2D}, C_q and C_{it} definitions cited before. Thus, initially *ΔN1A* is extracted as:

$$\Delta N1A = \frac{KTN_{ST}e^2}{WL_{eff}^2}\int_{u_d}^{u_s}\frac{L_{eff}}{C_{dq}U_T^2 Cgvcu}\frac{1-e^{-u}}{(1-e^{-u}+C2)}du \approx \frac{KTN_{ST}e^2}{WL_{eff}C_{dq}U_T^2 Cgvc}\int_{u_d}^{u_s}\frac{1}{u+c2(1+u)}du \quad \text{(S24)}$$

where *1-e^{-u}≈u/(1+u)* approximation is considered in order to obtain an analytical solution while *C2=(C+C$_{it}$)/C$_{dq}$*. The accuracy of the applied approximation is presented in Fig. S2a for a wide range of *u* values where the *IV* parameters used are from the DUT measured in the present study (cf. row 3 of Table S1 in Section S.6), but identical performance is obtained if other parameters sets are used.[33, 35, 38, 40, 42-43, 49] Then *ΔN1B* is derived:

$$\Delta N1B = \frac{KTN_{ST}e^2\mu}{WL_{eff}^2 v_{sat}CC_{dq}U_T}\int_{u_s}^{u_d}\left(\frac{1-e^{-u}}{u(1-e^{-u}+C2)}\right)^2|du| \approx \frac{KTN_{ST}e^2\mu}{WL_{eff}^2 v_{sat}CC_{dq}U_T}\int_{u_s}^{u_d}\left(\frac{1}{u+c2(1+u)}\right)^2 \quad \text{(S25)}$$

where again *1-e^{-u}≈u/(1+u)* is accurately considered (cf. Fig. S2b). Afterwards *ΔN3B* is estimated as:

$$\Delta N3B = \frac{2KTN_{ST}e^2\alpha_c\mu^2}{WL_{eff}^2 v_{sat}C}\int_{u_s}^{u_d}\frac{1-e^{-u}}{u(1-e^{-u}+C2)}|du| \approx \frac{2KTN_{ST}e^2\alpha_c\mu^2}{WL_{eff}^2 v_{sat}C}\int_{u_s}^{u_d}\frac{1}{u+c2(1+u)}|du| \quad \text{(S26)}$$

which ends up in the same integral as in *ΔN1A* case thus, it is solved similarly.
Regarding Mobility Fluctuation effect (*Δμ*), local *Δμ 1/f* noise is calculated as:[27 (Equation 6.75)]

$$\frac{S_{\delta I_n^2}}{I_D^2}f|_{\Delta\mu} = \frac{\alpha_H e}{|Q_{2D}|W\Delta x} \quad \text{(S27)}$$

Total *Δμ 1/f* noise normalized with squared drain current can be derived from Equations S12, S15 and S27:

$$\frac{S_{I_D}}{I_D^2}f|_{\Delta\mu} = \frac{\alpha_H e}{WL_{eff}^2}\int_0^L\frac{1}{|Q_{2D}|}dx = \frac{\alpha_H e}{WL_{eff}^2}\int_{u_s}^{u_d}\frac{1}{|Q_{2D}|}\left[-|Q_{2D}|\frac{L_{eff}}{CU_T gvc}\frac{C_q + C_{it} + C}{C_q} - \frac{\mu}{v_{sat}}\frac{C_{dq}U_T|du|}{C}\right]du \quad \text{(S28)}$$

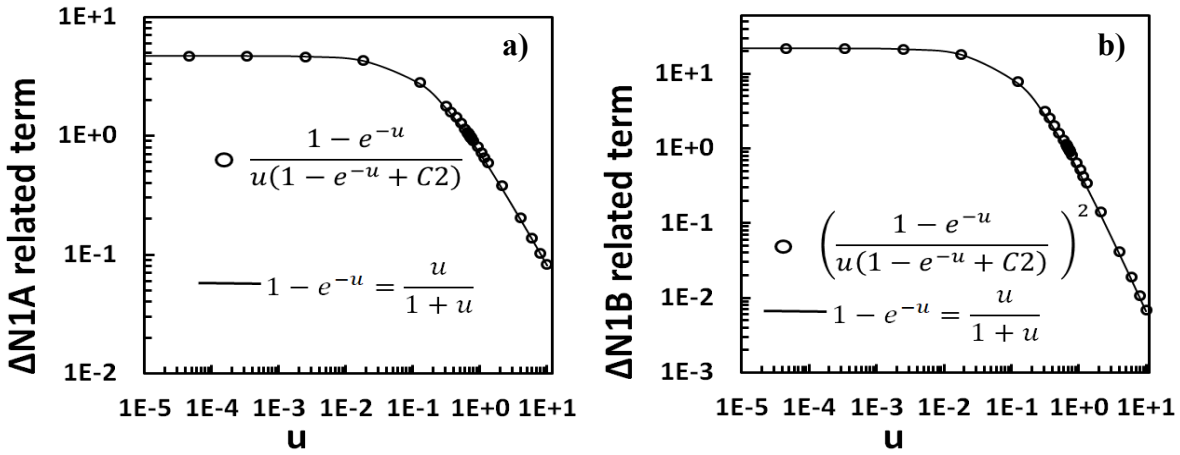

Fig. S2. *1/f* noise *ΔN1A* (a) and *ΔN1B* (b) related terms vs. *u* where markers represent the original derived expression and lines the $1\text{-}e^{-u}\approx u/(1+u)$ approximation.

where α_H is the unitless Hooge parameter used as *Δμ 1/f* noise model parameter. The integral in Equation S28 is divided into two integrals as *Δμ=ΔμA-ΔμB*:

$$\Delta\mu A=\frac{\alpha_H e}{WL_{eff}^2}\int_{u_d}^{u_s}\frac{1}{|Q_{2D}|}\left[|Q_{2D}|\frac{L_{eff}}{CU_T gvc}\frac{C_q+C_{it}+C}{C_q}\right]du=\frac{\alpha_H e}{WL_{eff}CU_T gvc}\int_{u_d}^{u_s}\frac{1-e^{-u}+C2}{1-e^{-u}}du \quad \text{(S29a)}$$

$$\Delta\mu B=\frac{\alpha_H e}{WL_{eff}^2}\int_{u_s}^{u_d}\frac{1}{|Q_n|}\left[\frac{\mu}{v_{sat}}\frac{C_{dq}U_T}{C}\right]|du|=\frac{\alpha_H e\mu}{CWL_{eff}^2 v_{sat}}\int_{u_s}^{u_d}\frac{1}{u}|du| \quad \text{(S29b)}$$

For the *ΔR 1/f* noise model cited in Equation 11 of the main manuscript, source and drain transconductances are calculated as:

$$g_{ms,d}=\frac{\partial I_D}{\partial u_{s,d}}\frac{\partial u_{s,d}}{\partial V_{cs,d}}\frac{\partial V_{cs,d}}{\partial V_{gs}}=\frac{\mu_{eff}WC_{dq}U_T^2}{L}\left[(C_{dq}+C+C_{it})u_{s,d}+(C+C_{it})e^{-u_{s,d}}\right]\frac{1-e^{-u_{s,d}}}{U_T}\frac{C_{t,}}{C+C_{it}+C_{dq}} \quad \text{(S30)}$$

SECTION S.4 *IV* parameter extraction procedure

Fundamental *IV* parameters such as *μ*, V_{GBO}, N_{it}, V_{it} and R_{CA} are extracted from low V_{DS} regime. In more detail, $\mu=g_{mmax}L/(V_{DS}.W.C_b)$[65] where g_m is the device transconductance while N_{it}, V_{it} are derived from the subthreshold slope $SS=(C_{itSS}/C_b+1)U_T ln(10)$[40, 46] where in subthreshold region, interface trap capacitance is approximated as $C_{itSS}=n_{it}.e/U_T$[40, 46] and n_{it} is the interface trap density which is related with N_{it}, V_{it} parameters as $n_{it}=N_{it}/(1+e^{(-Vc-Vit)/UT})$.[63] Then, V_{GBO}, R_{CA} can be obtained by fitting the model with experiments at low and high I_D regime, respectively. Parameters such as n_{DIBL}, u_{sat}, *λ*, can be estimated from high V_{DS} region if sufficient experiments are available. Thus, n_{DIBL} is zero when there is not a V_{DS} dependence of measured V_{TH}[33, 35, 38, 40, 42-43] while it is adjusted appropriately to capture this V_{DS} dependence in case it is noticed.[49, 65] u_{sat} is derived from high $V_{GS(B)}$[55] with values around 5.10^5-5.10^6 *cm/s* in agreement with bibliography for every case while in some occasions, CLM is observed usually in output characteristics and thus, *λ* is extracted.[33, 38, 40, 42] Finally in the DUT under test[65] where

intermediate V_{DS} values are also included in the measurement setup, the extraction of the above parameters for low (*0.1-0.2 V*) and high (*0.9-1 V*) V_{DS} does not provide an acceptable fitting for the rest of V_{DS} points and thus V_{DS}- dependent R_{CB}, *bRC* parameters are adjusted in order to achieve a remarkable performance of the *IV* model for every V_{DS} region.

SECTION S.5 *IV* and *1/f* noise plots of 2D-FETs

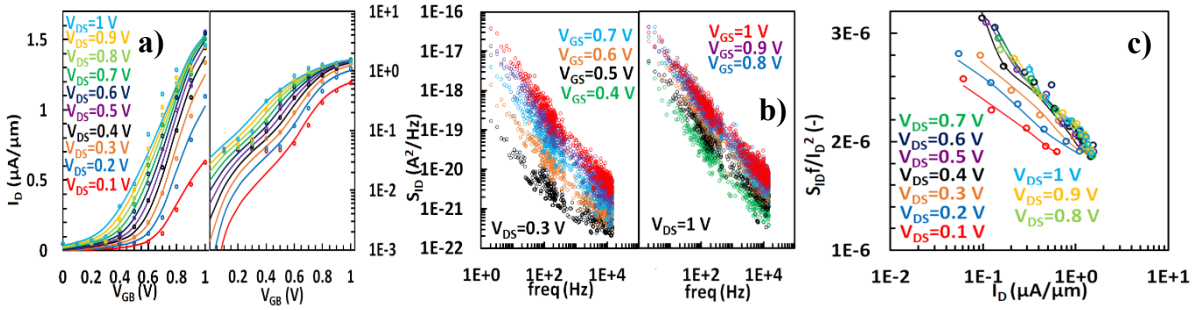

Fig. S3. a) Transfer characteristics at drain voltage V_{DS}=*0.1* to *1 V* (step *0.1 V*) at linear (left subplot) and logarithmic (right subplot) y-axis, b) Relative Power Spectral Density (PSD) of drain current noise S_{ID} for back-gate voltage V_{GB}=*0.4* to *1 V* (step *0.1 V*) at V_{DS}=*0.3*, *1 V* (left, right subplot, respectively) and c) $S_{ID}f/I_D^2$ vs. normalized drain current I_D at V_{DS}=*0.1* to *1 V* (*0.1 V* step) for Li-ion glass substrate SL MoS_2 FET[65] with width *W=4 μm* and length *L=1 μm*. Markers: measurements, lines: model.

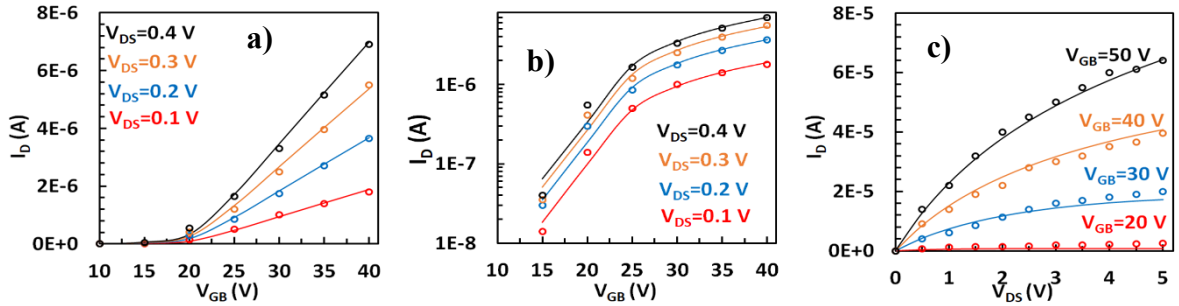

Fig. S4. I_D vs. V_{GB} at a) linear, b) logarithmic y-axis at V_{DS}=*0.1*, *0.2*, *0.3* and *0.4 V* and c) vs. V_{DS} at V_{GB}=*20*, *30*, *40* and *50 V* for 10-layer $MoSe_2$ FET[38] with *W=2 μm* and *L=2 μm*. Markers: measurements, lines: models.

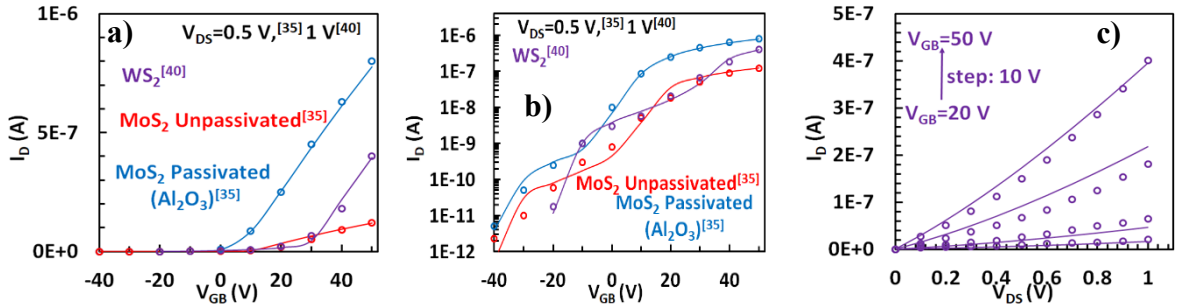

Fig. S5. I_D vs. V_{GB} at a) linear and b) logarithmic y-axis for Al_2O_3 passivated (blue) and unpassivated (red) single-layer (SL) MoS_2 FET[35] with *W=1 μm* and *L=0.4 μm* at V_{DS}=*0.5 V* and for a SL WS_2 FET[40] (magenta) with *W=27 μm* and *L=2 μm* at V_{DS}=*1 V*. c) I_D vs. V_{DS} for the WS_2 FET[40] at V_{GB}=*20*, *30*, *40* and *50 V*. Markers: measurements, lines: models.

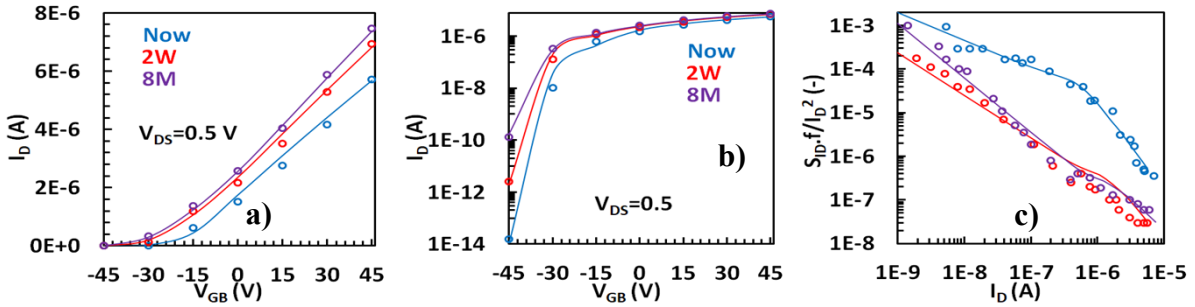

Fig. S6. I_D vs. V_{GB} at a) linear, b) logarithmic y-axis and c) output noise divided by squared drain current $S_{ID}f/I_D^2$ vs. I_D for a SL MoS_2 FET[43] exactly (blue), 2 weeks (red) and 8 months (magenta) after fabricated and placed in vacuum system with *W=10 µm* and *L=25 µm* at V_{DS}*=0.5 V*. Markers: measurements, lines: model.

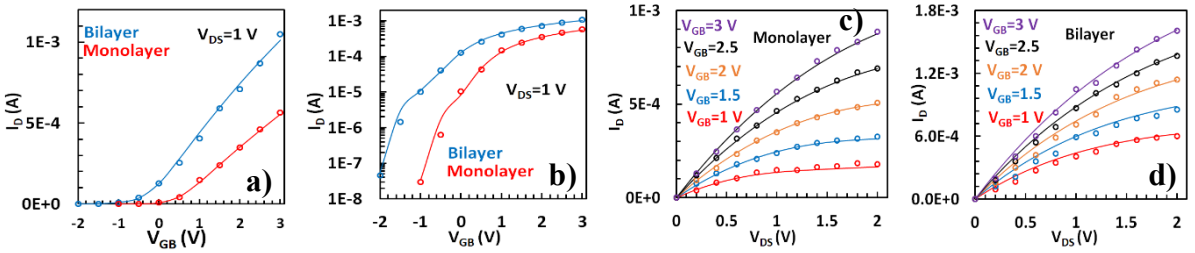

Fig. S7. I_D vs. V_{GB} at a) linear, b) logarithmic y-axis for bilayer (BL) (blue) and SL (red) MoS_2 FET[49] with *W=15 µm* and *L=0.3 µm* at V_{DS}*=1 V* and I_D vs. V_{DS} for c) the SL and d) the BL device at V_{GB}*=1*, *1.5*, *2*, *2.5* and *3 V*. Markers: measurements, lines: models.

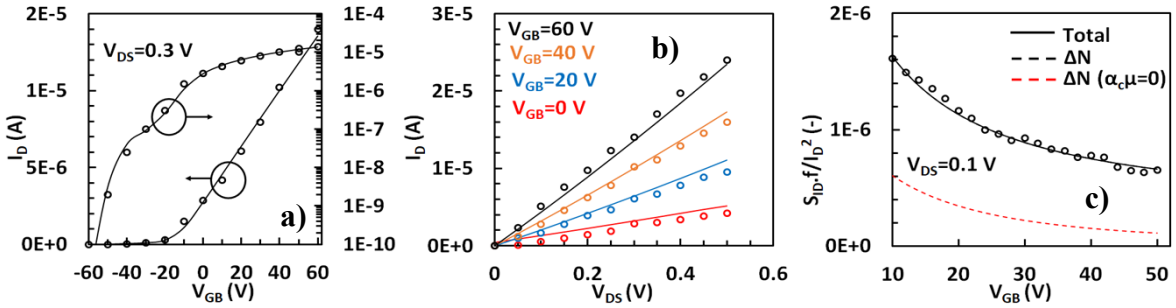

Fig. S8. I_D vs. a) V_{GB} in linear (left) and logarithmic (right) y-axis for V_{DS}*=0.3 V*, vs. b) V_{DS} for V_{GB}*=0*, *20*, *40* and *60 V* and c) $S_{ID}f/I_D^2$ vs. V_{GB} at V_{DS}*=0.1 V* for a SL MoS_2 FET[33] with *W=3.32 µm* and *L=1.71 µm*. Markers: measurements, solid lines: model, dashed lines: Carrier number fluctuation *ΔN* model with (black) and without (red) *CMF* effect ($\alpha_c\mu$).

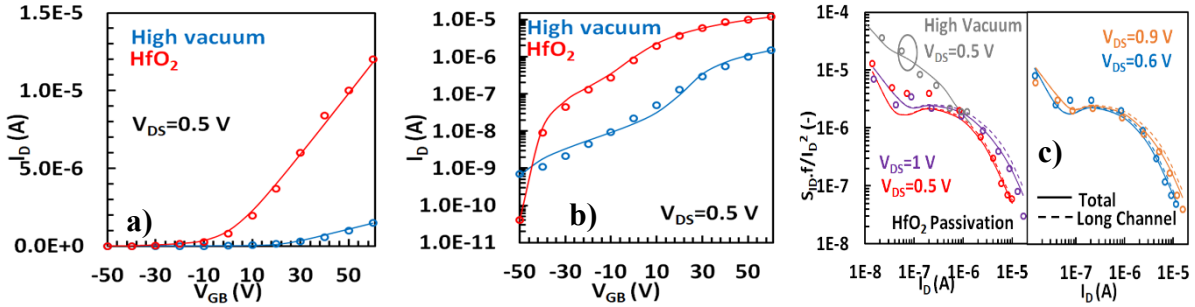

Fig. S9. I_D vs. V_{GB} at a) linear, b) logarithmic y-axis at V_{DS}*=0.5 V* at high vacuum (blue) and after HFO_2 passivation (red) and c) $S_{ID}f/I_D^2$ vs. I_D after HFO_2 passivation at V_{DS}*=0.5* (red), *0.6* (blue), *0.9* (orange) and *1 V* (magenta), for a 7-layer $MoTe_2$ FET[42] with *W=5.5 µm* and *L=2 µm*. $S_{ID}f/I_D^2$ is also shown at high vacuum case (grey) at V_{DS}*=0.5 V*. Markers: measurements, lines: models, dashed lines: long channel model.

SECTION S.6 Tables with *IV* and *1/f* noise model parameters

Table S1. *IV* Model Parameters

Param	W	L	C	μ	V_{GBO}	n_{DIBL}	u_{sat}	N_{it}	V_{it}	R_{CA}	R_{CB}	b_{Rc}	λ
Units	μm	μm	μFcm^{-2}	$cm^2(Vs)^{-1}$	V	-	cm/s	cm^{-2}	eV	Ω	Ω/V	-	1/V
[64]	4	1	2.17	20	0.26	0.45	2.10^4	$6.5.10^{12}$	0.117	4871	$6.3.10^4$	1.29	0
[38]	2	2	0.0384	27	5.43	0	4.10^3	$3.6.10^{12}$	0.14	1.10^3	0	1	0.05
[35] Unpas	1	0.4	0.0121	0.25	-40	0	1.10^4	$3.8.10^{12}$	0.2	4.10^5	0	1	0
[35] Al_2O_3	1	0.4	0.41	1.5	-32	0	1.10^4	$2.5.10^{12}$	0.21	$4.5.10^4$	0	1	0
[40]	27	2	0.0115	0.18	-20	0	1.10^4	$3.95.10^{12}$	0.155	6.10^5	0	1	0.95
[49]-1L	15	0.3	11.2	5.4	-0.72	0.18	1.10^4	6.10^{12}	0.09	120	0	1	0
[49]-2L	15	0.3	11.2	10	-1.55	0.35	8.10^3	8.10^{12}	0.08	120	0	1	0
[43] Now	10	25	0.0115	43	-44.55	0	1.10^4	$1.9.10^{12}$	0.14	$3.5.10^3$	0	1	0
[43] 2W	10	25	0.0115	54	-44.68	0	1.10^4	2.10^{12}	0.08	4.10^3	0	1	0
[43] 8M	10	25	0.0115	61	-44.82	0	1.10^4	$2.2.10^{12}$	0.07	4.10^3	0	1	0
[33]	3.32	1.71	0.0115	27	-59.7	0	2.10^4	$3.3.10^{12}$	0.145	500	0	1	0.3
[42] H. Vac.	5.5	2	0.0115	2.4	-57	0	8.10^3	$5.7.10^{12}$	0.153	120	0	1	0.06
[42] HFO_2	5,5	2	0.45	12	-40	0	4.10^3	$2.33.10^{12}$	0.11	120	0	1	0.35

Table S2. *1/f* noise Model Parameters

Param	N_{ST}	α_C	α_H	$S_{\Delta R}{}^2$
Units	$eV^{-1}cm^{-2}$	V.s/C	-	Ω^2HZ^{-1}
[64]	1.10^{11}	$1.61.10^6$	3.10^{-3}	0
[38]	$1.35.10^{10}$	$1.35.10^6$	$1.3.10^{-3}$	50
[35] Unpas	4.10^{11}	510^7	$1.8.10^{-2}$	0
[35] Al_2O_3	5.10^{10}	1.10^3	$1.4.10^{-3}$	0
[40]	8.10^{12}	5.10^7	0.12	0
[49]-1L	1.10^{13}	1.10^3	9.10^{-2}	0
[49]-2L	9.10^{12}	1.10^3	$1.3.10^{-3}$	0
[43] Now	1.10^{15}	1.10^3	1.10^{-5}	0
[43] 2W	4.10^{13}	1.10^3	1.10^{-5}	0
[43] 8M	3.10^{13}	1.10^4	1.10^{-5}	0
[33]	4.10^{12}	9.10^4	1.10^{-5}	0
[42] H. Vac.	$5.5.10^{12}$	1.10^6	0.13	0
[42] HFO_2	3.10^{12}	1.10^3	6.10^{-4}	0

Extracted *IV* parameters of the measured DUT[65] (μ, V_{GBO} and R_C), derived here, are akin to those presented in Ref. 65 while trap-related ones (N_{it} and V_{it}) vary, which can be justified by the different measurement conditions which are probable to induce additional trap effects. Regarding the extracted 1/f noise parameter, N_{ST} is similar[36] or lower than other SL to FL MoS_2 FETs reported in literature[37, 43, 46, 49] while the strong α_c (in comparison with values in the range of 1.10^3-1.10^4 *Vs/C* reported in MOSFETs[23, 27 (Section 6.3)]) has been already recorded in similar 2D-FETs.[35] Extracted α_H is also close[35,38] or decreased[40, 49] in comparison with literature. Besides, for the $MoSe_2$ FET of Ref. 38, a low N_{ST} and a significant α_c are recorded while α_H is relatively close to the value reported in the initial study. Furthermore, as far as the devices of Refs 35, 40 are concerned, N_{ST}, α_H are larger in WS_2 device with the unpassivated MoS_2 to follow and the top-passivated to demonstrate the lower values. Note that the passivated SL MoS_2 FET does not display a significant *CMF* effect in contrast to the other two devices which present an equivalently strong $\alpha_c\mu$ product. N_{ST}, α_c parameters extracted here are similar with those in Ref. 40 for the WS_2 device while no information regarding these parameters is provided in Ref. 35 for the MoS_2 FETs under discussion. The simplified $(1+\alpha_C\mu C_{t,b} I_D/g_m)^2(g_m/I_D)^2 \Delta N$ model (uniform channel approximation), which is applied in both Refs 35, 40, is not accurate for the unpassivated MoS_2 FET[35] while even though it fits acceptably the data for the passivated MoS_2 FET[35] and the WS_2 FET,[40] it is validated for only one V_{DS} value. Regarding the devices of Refs 43, 49, α_C is imperceptible everywhere while HFLaO (SL-BL) MoS_2 FETs exhibit a quite reduced (*2* decades) N_{ST} parameter in comparison with the just fabricated SiO_2 SL MoS_2 FET confirming that the high-k dielectric presents weaker trapping effects. α_H parameter has a moderate effect on high-k dielectric FETs while it is negligible in SiO_2 devices. N_{ST} parameter extracted here for both HFLao[49] and SiO_2[43] 2D-FETs, is quite close to the values recorded in Refs 43, 49, respectively, where again a simplified $(g_m/I_D)^2 \Delta N$ model is applied. Finally, for the device of Ref. 33, an intense N_{ST} is recorded which dominates *1/f* noise with a moderate contribution from α_c while α_H is negligible.